

Controlling Moisture for Enhanced Ozone Decomposition: A Study of Water Effects on CeO₂ Surfaces and Catalytic Activity

Suchitra Gupta,[†] Joon Hwan Choi,[‡] Hojin Jeong,^{*,‡} Seung-Cheol Lee,^{*,†} and
Satadeep Bhattacharjee^{*,†}

[†]*Indo-Korea Science and Technology Center (IKST), Bangalore-560064, India*

[‡]*Functional Ceramics Department Korea Institute of Materials Science (KIMS) 797
Changwon-daero, Seongsan-gu, Chanwon-si, Gyeongsangnam-do, 51508, South Korea*

E-mail: hjeong@kims.re.kr; leesc@kist.re.kr; s.bhattacharjee@ikst.res.in

Abstract

This study investigates the catalytic degradation of ground-level ozone on low-index stoichiometric and reduced CeO₂ surfaces using first-principles calculations. The presence of oxygen vacancies on the surface enhances the interaction between ozone and catalyst by serving as active sites for adsorption and decomposition. Our results suggest that the {111} surface has superior ozone decomposition performance due to unstable oxygen species resulting from reaction with catalysts. However, when water is present, it competes with ozone molecules for these active sites, resulting in reduced catalytic activity or water poisoning. A possible solution could be heat treatment that reduces the vacancy concentration, thereby increasing the available adsorption sites for ozone molecules while minimizing competitive adsorption by water molecules. These results suggest that controlling moisture content during operation is crucial for the efficient use of CeO₂-based catalysts in industrial applications to reduce ground-level ozone pollution.

Keywords

Ozone decomposition, water poisoning, chemisorption, first-principles calculations

1 Introduction

Ozone exhibits antibacterial and antiviral properties and has a redox potential of 2.08 eV, making it a powerful oxidizing agent. These properties pave the way for applications such as water purification, pollutant degradation and inhibition of nitric acid production by fully oxidizing exhaust gases.¹⁻⁴ This leads to the release of residual ozone in the atmosphere at ground level, which can negatively impact human health and damage crops.^{2,5-10} In the interests of human and environmental safety, reducing ozone pollution in industrial processes and in the atmosphere is of the utmost importance. Activated carbon adsorption, chemical absorption, and catalytic decomposition are the existing processes to remove the ground level ozone.¹¹⁻¹⁴ Among which catalytic decomposition of ozone into O_2 at low temperatures is the promising method of ozone elimination as it gives better efficiency and is also environment friendly process. Transition metal oxides and noble metal catalysts are the commonly used catalysts for ozone decomposition. Owing to the high cost of noble metals, transition metal oxides have attracted greater interest in the past. It has been found that *p*-type oxides like MnO_2 , NiO , Co_3O_4 , Fe_2O_3 , Ag_2O , and CeO_2 shows greater catalytic efficiency as compared to the *n*-type oxides which include V_2O_5 , CuO , MoO_3 etc.¹⁵

Ozone can be adsorbed on metal oxide surfaces and dissociate into the reactive oxygen species, however, the oxide surfaces have a high affinity for water molecules.^{16,17} The oxide surface is hydroxylated by the chemical adsorption and dissociation of water. Depending on the surface structure, isolated hydroxyl groups, hydrogen-bonded hydroxyl groups, and bridged hydroxyl groups can be formed on different oxides.^{18,19} This can greatly affect the catalytic decomposition of ozone on oxides. Previous studies claim that surface hydroxyl groups are the site of ozone depletion, however, not all hydroxyl groups are catalytically active.^{20,21} The presence of water has a major impact on the catalyst efficiency for ozone decomposition in transition metal oxides.^{17,22-24}

In this work, using first-principles calculation we have studied the interaction of ozone on $\{111\}$, $\{110\}$, and $\{100\}$ surfaces of CeO_2 . Due to differences in the atomic arrangement, these surfaces exhibit different catalytic performances. As oxygen vacancies are the adsorption sites for ozone decomposition and their presence has also improved the rate of ozone elimination in oxides. In the presence of oxygen vacancies, ozone behavior on the considered surfaces was also analyzed. It has already been pointed out that the presence of water interferes with the catalytic activity of the catalyst, we have looked into the effect of water on ozone adsorption on stoichiometric and oxygen-deficient $\text{CeO}_2\{111\}$ surface. We have also shown the effect of oxygen vacancies concentration on the adsorption of ozone in the presence of water. Furthermore, we investigate the competitive co-adsorption of H_2O and O_3 on CeO_2 surfaces, examining their binding properties and potential interference with ozone decomposition. We find that heat treatment may help optimize the performance of CeO_2 -based catalysts in the dissociation of ground-level ozone. Heat treatment can reduce the number of oxygen vacancies on CeO_2 surfaces, making the surface more similar to a stoichiometric surface with no defects. However, as H_2O has larger adsorption energy on reduced $\{111\}$ surfaces compared to its adsorption energies on stoichiometric $\{111\}$, $\{110\}$, and $\{100\}$ surfaces, therefore, by reducing oxygen vacancies, the surface becomes not only more stable, it also becomes less reactive towards H_2O , which can improve the selectivity of ozone dissociation in the presence of water.

2 Computational Details

Our first-principles calculations are based on density functional theory as implemented in the Vienna Ab initio Simulation Package (VASP).²⁵ The exchange-correlation energy is implemented by the Perdew-Burke-Ernzerhof (PBE),²⁶ and the core-valence electron interaction is described using the projected augmented wave (PAW) method.²⁷ For Ce f orbitals we have chosen U value of 5 eV throughout the calculations in consistent with the values recommended in previous theoretical studies.²⁸⁻³¹ The $\{111\}$, $\{110\}$, and $\{100\}$ slabs are constructed using (1×1) , (2×1) ,

and (2×2) conventional unit cells consisting of 12 (16 CeO₂ units), 4 (16 CeO₂ units), and 7 atomic layers (24 CeO₂ units) respectively. A vacuum gap of at least 12 Å is included along the z-direction to minimize the interaction between periodic images. The energy cut-off of 520 eV is used to truncate the plane wave basis sets and the entire Brillouin zone is sampled using $4 \times 4 \times 1$ k-points mesh. The spin-polarized calculations are carried out for a reduced system consisting of oxygen vacancies. The bottom layers are kept fixed, and the uppermost layers are allowed to relax until the maximum forces on each atom are less than 0.03 eV/Å. The dipole correction is applied along the z-direction to treat the artificial electric field arising due to the asymmetry (resulting due to adsorbate adsorption and introduction of oxygen vacancies) and periodicity of the slab.

3 Results and Discussion

CeO₂ crystallizes in the cubic fluorite structure with $Fm\bar{3}m$ symmetry, and the slabs are modelled using the lattice constant of 5.49 Å obtained theoretically which is in close agreement with the experimental value of 5.41 Å³² and previous theoretical results.^{29,33–35} We have investigated the {111}, {110}, and {100} surfaces of CeO₂, among which {100} surface is type III according to Tasker classification i.e. it is polar.³⁶ For the simulation of {100} surface, we have moved the half of surface oxygen atoms to the other side of the slab to quench the dipole moment normal to the surface. CeO₂{111} surface is most stable of all followed by {110}, and {100} surfaces.^{37,38} O atoms of ozone, water, and surfaces are represented by O_{ozone} , O_{water} , and O respectively.

In the following sections, we explore the adsorption and decomposition of ozone (O₃) on CeO₂ surfaces and the influence of surface structure and moisture on the catalytic activity of CeO₂-based catalysts. We find that O₃ adsorbed in a dissociative form is more thermodynamically favorable on the {111} surface compared to {110} and {100} surfaces. Oxygen vacancies on the reduced surfaces of CeO₂ serve as active sites for O₃ adsorption and decomposition, facilitating the process more efficiently than on stoichiometric surfaces. Additionally, the presence of water interferes with O₃ adsorption on reduced {111} surfaces by blocking the oxygen-deficient site, which is crucial

for ozone adsorption and decomposition. These findings contribute to our understanding of ozone decomposition on CeO₂ catalysts and offer insights for optimizing their performance in various industrial applications.

3.1 O₃ adsorption on stoichiometric {111}, {110}, and {100} surfaces

We have considered the adsorption of O₃ on the stoichiometric CeO₂ surfaces and calculated the adsorption energy ($E_{ads.}$) using the following relation:

$$E_{ads.} = E_{slab+molecule} - E_{slab} - E_{molecule}, \quad (1)$$

where, $E_{slab+molecule}$ is the energy of slab with molecule adsorbed on it, E_{slab} and $E_{molecule}$ are the energies of clean slab and molecule in the gaseous phase respectively.

O₃ gets adsorbed at Ce site of {111} surface forming a Ce-O_{ozone} bond of length 2.66 Å with an adsorption energy of -0.40 eV (Figure 1(a)). As a result of interaction, we notice an elongation in the O_{ozone} - O_{ozone} bond length from 1.28 Å in the gaseous phase to 1.32 Å in the adsorbed state. The oxygen atom not bound to the surface atoms has O_{ozone} - O_{ozone} bond length of 1.29 Å. Whereas, on {110} surface O₃ binds with an adsorption energy of -0.91 eV and forms a bond with two Ce atoms of length 2.60 Å resulting in an elongation of O_{ozone} - O_{ozone} bond to 1.33 Å (Figure 1(b)). On {100} surface, O₃ binds to the surface through Ce atoms forming a Ce-O_{ozone} bond of lengths 2.61-2.63 Å and the corresponding adsorption energy is -1.04 eV (Figure 1(c)). Interestingly, compared to other surfaces elongation in O_{ozone}-O_{ozone} bond is maximum on {100}, the bond length is 1.36 Å after interaction with the surface. There is a decrease in the bond angle of O₃ upon interaction with the CeO₂ {111} and {100} surfaces and it slightly increases for {110} surface (see Table 1). The reduction in the bond angle of ozone is more prominent in {100} and can be attributed to the increased O_{ozone}-O_{ozone} bond length which leads to the weaker repulsion. Also, the increase in the bond length of ozone will reduce the bond dissociation energy and facilitate further reactions.

The charge density difference ($\delta\rho$) is calculated using the following relation:

$$\delta\rho = \rho_{slab+O_3} - \rho_{slab} - \rho_{O_3} \quad (2)$$

where, ρ_{slab+O_3} , ρ_{slab} , and ρ_{O_3} are the charge density of slab with O_3 adsorbed on it, the CeO_2 surface and the isolated O_3 molecule in its adsorbed configuration respectively. The charge density difference analysis shows the accumulation of electrons in Ce-O bond and depletion on the surface Ce atoms which indicate the electron transfer from the surface to O_3 (see Figure 1(d)-(f)). Also, we notice a charge depletion around one of the oxygen atoms of ozone indicating that it donates electrons to the other two oxygen atoms of ozone as well. The Bader charge analysis shows the transfer of electrons from the surface to the molecule. The electron transfer is maximum on $\{100\}$ surface followed by $\{110\}$ and $\{111\}$ surface indicating that O_3 interacts strongly with $\{100\}$ surface which is also reflected in the adsorption energy values. In a nutshell, O_3 becomes negatively charged with the changed bond angle and elongated $O_{ozone}-O_{ozone}$ bond length upon adsorption on CeO_2 surfaces. The structural parameters and adsorption energies are summarised in Table 1.

3.2 O_3 dissociation on stoichiometric $\{111\}$, $\{110\}$, and $\{100\}$ surfaces

The adsorption energies of dissociative adsorption of O_3 on stoichiometric CeO_2 surfaces are -0.15 eV, -1.31 eV, and -1.46 eV for the $\{111\}$, $\{110\}$, and $\{100\}$ surfaces respectively. The lowest energy geometries of dissociative O_3 on CeO_2 surfaces are shown in Figure S1 of supplementary information. O_3 dissociates into O_2-O and the dissociation occurs during minimization. On $\{111\}$ surface, O_2 gets attached to the surface Ce atom forming two Ce- O_{ozone} bonds of length 2.54 Å and 2.47 Å and other O_{ozone} atom binds with the surface O and Ce atoms, the corresponding bond lengths are 1.40 Å and 2.55 Å respectively (Figure S1(a) of supplementary information). At $\{110\}$ surface, O_2 (of O_3) forms a single Ce- O_{ozone} bond of length 2.37 Å and O gets attached to the surface Ce and O atoms forming a bond of length 2.46 Å and 1.37 Å respectively (Figure S1(b) of

supplementary information). Whereas, on {100} surface O₂ (of O₃) forms Ce-O bond of lengths 2.48-2.68 Å. O (of O₃) gets attached to two Ce atoms and the surface oxygen atom (Figure S1(c) of supplementary information). The structural parameters and binding energies are given in Table S1 of supplementary information.

O₃ dissociation is thermodynamically more favorable on {110} and {100} surfaces as compared to the {111} surface. However, the oxygen species formed as a result of ozone decomposition should not get stabilised on the surface. This will make it difficult for the species to leave the surface and the adsorption sites won't be available to carry out further reaction. As per the adsorption energy, oxygen species formed as a result of ozone decomposition is quite stable on {110} and {100} surfaces as compared to {111} which makes {111} surface more suitable for ozone decomposition.

3.3 O₃ adsorption on reduced {111}, {110}, and {100} surfaces

As oxygen vacancies act as an active site for ozone adsorption and decomposition, we have introduced the oxygen vacancies of concentrations 0.25, 0.125, and 0.125 on {111}, {110}, and {100} surfaces respectively. At {111} and {110} surfaces, O₃ occupy the oxygen deficient site with an adsorption energy of -3.24 eV and -2.65 eV respectively (Figure 2(a) and (b)). Whereas, on {100} surface O₃ binds to Ce atoms slightly away from the oxygen-deficient site, its adsorption energy is -2.71 eV (Figure 2(c)). The binding energies and structural parameters are tabulated in Table 2. We notice a significant elongation in O_{ozone}-O_{ozone} bond length on reduced surfaces as compared to the stoichiometric. This indicates that the presence of oxygen vacancies facilitate the decomposition more efficiently as compared to the stoichiometric surfaces.

Considering the dissociative adsorption of O₃ on reduced CeO₂ surfaces we find that O₃ adsorbed in dissociative form is thermodynamically more favorable on {111} surface as compared to {110} and {100} surfaces (see Table S2 of supplementary information). O₃ dissociates into O₂-O on {111} surface with O_{ozone} atom occupying the oxygen-deficient site and O₂ (of O₃) gets stabilized at 3.04 Å from the surface (Figure 3(a)). It clearly shows the release of oxygen gas

after O_3 dissociation. Contrary to $\{111\}$ surface, O_2 of O_3 occupies the oxygen deficient site and O_{ozone} binds with the surface O and Ce atoms on both $\{110\}$ and $\{100\}$ surfaces (Figure 3(b) and (c)). The adsorption energies of O_3 on reduced CeO_2 surfaces reveal that the binding becomes stronger in the presence of oxygen vacancies. On $\{111\}$ surface of reduced CeO_2 , oxygen gas is released spontaneously after dissociation which make it a good candidate for ozone decomposition as compared to $\{110\}$ and $\{100\}$ surfaces in the presence of oxygen vacancies.

3.4 H_2O adsorption on stoichiometric $\{111\}$, $\{110\}$, and $\{100\}$ surfaces

The presence of H_2O affect the catalytic activity of O_3 decomposition on the oxide surfaces. We have obtained the most stable adsorption site of H_2O both in associative and dissociative state on $\{111\}$, $\{110\}$, and $\{100\}$ surfaces. The adsorption energies and structural geometries are tabulated in Table S3 of supplementary information. The adsorption energies of H_2O adsorbed in the associative form are -0.54 eV, -0.77 eV, and -0.92 eV on $\{111\}$, $\{110\}$, and $\{100\}$ surfaces respectively. H_2O interacts strongly with $\{100\}$ surface and weakly with $\{111\}$ surface, similar trend was also observed for O_3 adsorption. The interaction of H_2O with $\{111\}$ surface is slightly stronger in comparison to O_3 whereas, on $\{110\}$ and $\{100\}$ surfaces O_3 interaction is stronger than the H_2O . H_2O prefers to adsorb at Ce site forming a Ce- O_{H_2O} bond of length 2.61 Å and 2.65 Å on $\{111\}$ and $\{110\}$ surfaces respectively (Figure S2(a) and (b) of supplementary information). We notice the formation of one hydrogen bond of length 1.74 Å on $\{111\}$ surface, whereas H_2O forms two hydrogen bonds of length 2.00 Å on $\{110\}$ surface. Contrary to $\{111\}$ and $\{110\}$ surface, H_2O is shared between two Ce atoms forming a Ce- O_{H_2O} bond of length 2.65 Å on $\{100\}$ surface (Figure S2(c) of supplementary information).

The adsorption energies of H_2O adsorbed in dissociative form on $\{111\}$, $\{110\}$, and $\{100\}$ surfaces are -0.52 eV, -1.07 eV, and -1.69 eV respectively. OH binds to the Ce atom and H gets attached to the adjacent surface oxygen atom in the most stable configuration on $\{111\}$ and $\{110\}$ surfaces (Figure S2(d) and (e) of supplementary information). The adsorption energy difference between H_2O adsorbed in associative and dissociative form on $\{111\}$ surface is 0.02 eV suggesting

the co-existence of H₂O in both associative and dissociative state on {111} surface. At {100} surface, OH occupies the vacant site created as a result of the removal of half of the surface oxygen atoms and H gets attached to the surface oxygen atom (Figure S2(f) of supplementary information). The adsorption energies and structural parameters are given in Table S3 of supplementary information. Our adsorption energies and geometrical parameters are in close agreement with the previous theoretical studies done by Molinari et al.³¹

3.5 H₂O adsorption on reduced {111}, {110}, and {100} surfaces

The adsorption energies of H₂O adsorbed in associative form on reduced CeO₂ {111}, {110}, and {100} surfaces are -1.21 eV, -1.20 eV, and -1.00 eV respectively. H₂O forming bond with the surface Ce atom is the most stable binding configuration and there is a hydrogen bond formation on all the considered surfaces (see Figure S3(a)-(c) of supplementary information). In case of H₂O adsorbed in dissociative form, OH prefers to occupy the oxygen-deficient site and O_{water} gets attached to the surface oxygen atom. On {110} surface, OH forms a hydrogen bond of length 1.81 Å, there is no hydrogen bond formation on any other surfaces as shown in Figure S3(d)-(f) of supplementary information. The adsorption energies of both O₃ and H₂O are more negative on reduced CeO₂ surfaces indicating the strong interaction between vacancies and adsorbates. The results are in agreement with the previous work done by Molinari et al.,³¹ Fronzi et al.,³⁹ and Watkins et al.⁴⁰ However, the presence of oxygen vacancies favors the binding of O₃ as compared to that of H₂O. The adsorption energies and geometrical parameter are summarised in Table S4 of supplementary information.

3.6 Competition between H₂O and O₃ on CeO₂ {111} surface: Coadsorption study

From our previous results, it is clear that both O₃ and H₂O are strongly attracted to the surface and prefers same binding sites for adsorption. There will be competitive adsorption between O₃

and H₂O on the CeO₂ surfaces. As CeO₂{111} surface is the most stable surface of all, we have investigated the coadsorption of O₃ and H₂O on stoichiometric CeO₂{111} surface. We have looked into the effect of H₂O and H-OH on the adsorption of ozone as both H₂O and H-OH are equally probable on {111} surface. We have considered 2 × 2 conventional unit cells for the coadsorption of H₂O and O₃ on stoichiometric {111} surface. For a better comparison of O₃ adsorption energy in the presence and absence of H₂O, we have obtained the adsorption energy of O₃ on 2 × 2 conventional unit cells and got the adsorption energy of O₃ to be -0.43 eV. The adsorption energy is changed by 0.03 eV when the coverage of O₃ is reduced indicating that the O₃ coverage has a little effect on its binding on stoichiometric {111} surface of CeO₂. For the same coverage, the adsorption energy of H-OH is -0.64 eV, it is changed by 0.07 eV indicating that H-OH adsorption energy is coverage dependent as reported by Molinari *et al.*³¹ To look into the effect of H-OH on the adsorption energy of O₃ we varied the distance between O₃ and H-OH (see Figure 4(a)-(c)) and calculated the adsorption energy of O₃ using the following relation:

$$E_{ads.} = E_{slab+H-OH/H_2O+O_3} - (E_{slab+H-OH/H_2O} + E_{O_3}) \quad (3)$$

Where, $E_{slab+H-OH/H_2O+O_3}$, is the energy of H-OH/H₂O and O₃ adsorbed on slab, $E_{slab+H-OH/H_2O}$ is the energy of H-OH and H₂O adsorbed on slab and E_{O_3} is the energy of isolated O₃ in the gaseous phase. The adsorption energy of O₃ in the presence of H-OH is -0.26 eV when kept at a distance of 2.54 Å and its -0.43 eV in the absence of H-OH. Also, O₃ moves further away from the surface and binds at a distance of 2.75 Å (Ce-O_{ozone} bond length) from the surface in the presence of H-OH indicating weaker interaction between O₃ and surface (Table 3). This suggests that the presence of H-OH weakens the binding of O₃ on stoichiometric {111} surface. However, when O₃ is moved away from H-OH i.e. at a distance of 6.34 Å, there is a negligible interaction between H-OH and O₃, its adsorption energy is -0.38 eV which is close to its adsorption energy value of -0.43 eV in the absence of H-OH. At an intermediate distance of 3.98 Å, the binding energy of ozone is -0.27 eV indicating there is still an interaction between O₃ and H-OH. Charges and other structural

parameters of O₃ are similar to that in the absence of H-OH at 6.34 Å (see Table 3). O₃ becomes negatively charged and H-OH becomes slightly positively charged as a result of coadsorption.

We further calculated the charge density difference ($\delta\rho$) plot of two configurations in which O₃ is at distance of 2.54 Å and 6.34 Å from H-OH using the following relation:

$$\delta\rho = \rho_{slab+H-OH/H_2O+O_3} - \rho_{slab+H-OH/H_2O} - \rho_{O_3}, \quad (4)$$

where $\rho_{slab+H-OH/H_2O+O_3}$, $\rho_{slab+H-OH/H_2O}$, and ρ_{O_3} are the charge density of slab with H-OH/H₂O and O₃ adsorbed on it, the slab with H-OH/H₂O adsorbed on it, and the isolated O₃ molecule in its adsorbed configuration. We notice an electron accumulation along Ce-O_{ozone} bond and electron depletion on surface atoms suggesting the electron transfer from the surface to O₃. Also, there is a charge re-distribution on the H-OH when it is close to O₃ (at a distance of 2.54 Å), whereas it remains unaffected when it is moved further away from O₃ as shown in Figure 5(a) and (b). Our analysis confirms that there is an interaction between H-OH and O₃ when placed close to each other which clearly affects the binding and geometry of O₃ (see Table 3).

We also performed the analysis of H₂O and O₃ co-adsorption on {111} surface of CeO₂. The adsorption energy of H₂O for the same coverage is -0.57 eV. In the presence of H₂O, the binding energies of ozone obtained using equation 3 are -0.36 eV, -0.36 eV, and -0.39 eV when kept at a distance of 2.80 Å, 3.29 Å, and 6.57 Å respectively from H₂O (Figure 4(d)-(f)). There is a smaller change in the binding energies of ozone with its distance from H₂O suggesting that there is a negligible interaction between H₂O and O₃. We performed the Bader charge analysis for the two cases: one in which O₃ is at a distance of 2.80 Å and other at 6.57 Å from H₂O. There is an electron transfer from surface to O₃ molecule as per the Bader charge analysis (Table 4). Also, the charge density difference obtained using equation 4 reveals the electron accumulation along Ce-O_{ozone} bond and depletion along the surface Ce atom. There is no charge re-distribution on the H₂O irrespective of its distance from H₂O molecule which further confirms the negligible interaction between H₂O and O₃ (Figure 5(c) and (d)).

The effect of H-OH on O₃ adsorption energy is much more as compared to H₂O. This can be attributed to the strong interaction of H-OH with the surface as compared to the surface-H₂O interaction. As a result of which competitive adsorption between H-OH and O₃ weakens its interaction with the surface and hence the adsorption energy of O₃ becomes more positive in the presence of H-OH.

As per the adsorption energy, the H-OH is more favorable on reduced {111} surface as compared to H₂O and so we consider the coadsorption of O₃ and OH on reduced CeO₂ surface. In this case we are considering the effect of isolated hydroxyl group on ozone adsorption. For simulation of reduced CeO₂{111} surface we have considered 2 × 2 conventional unit cells and removed one oxygen atom introducing an oxygen vacancy of concentration 0.0625. Also, the adsorption energy of O₃ on {111} surface with vacancy concentration of 0.0625 in the absence of H₂O is -2.85 eV. O₃ prefers to occupy the oxygen deficient site in the absence of H₂O. In case of co-adsorption, there is one oxygen deficient site which gets occupied by OH. Since there is no available oxygen deficient site, O₃ binds to the surface Ce atom forming a Ce-O bond of length 2.45 Å (Figure 6(a)). There is a hydrogen bond formation between OH and O₃ of length 1.92 Å. The adsorption energy of O₃ in the presence of OH is calculated using the following relation:

$$E_{ads.}(O_3) = E_{slab+OH+O_3} - (E_{slab+OH} + E_{O_3}) \quad (5)$$

Where, $E_{slab+OH+O_3}$, is the energy of OH and O₃ adsorbed on a slab, $E_{slab+OH}$ is the energy of OH adsorbed on slab, and E_{O_3} is the energy of O₃ in the isolated gaseous phase. The adsorption energy of O₃ in the presence of OH is -1.58 eV i.e., its binding becomes less negative compared to its adsorption energy of -2.85 eV in the absence of H₂O. The stable binding geometry and geometrical parameters obtained because of coadsorption of O₃ and OH is shown in Figure 6(a) and tabulated in Table 5. We increased the concentration of oxygen vacancies to 0.125 on the surface by removing two surface oxygen atoms. In this case the adsorption energy of ozone in the absence of OH is -2.98 eV. OH occupies the oxygen deficient site and O₃ also has one deficient site

for adsorption. O_3 fills the vacancy site created as a result oxygen vacancy formation (see Figure 6(b)), its binding energy is -2.69 eV obtained using equation 5. In this case also, we do notice that the presence of OH weakens the interaction between O_3 and surface.

On the basis of above result we looked into the effects of hydroxylated surface on ozone adsorption. The adsorption energy of O_3 is calculated using the following relation:

$$E_{ads.}(O_3) = E_{slab+H+O_3} - (E_{slab+H} + E_{O_3}) \quad (6)$$

Where, $E_{slab+H+O_3}$ is the energy of O_3 adsorbed on hydroxylated slab, E_{slab+H} is the energy of hydroxylated slab, and E_{O_3} is the energy of O_3 in the isolated gaseous phase. On the hydroxylated surface, O_3 stays at the top of surface forming three hydrogen bonds of lengths 1.92, 1.86, and 1.78 Å (shown in Figure 7). Our results suggest that O_3 can not come closer to surface and forms chemical bond but the presence of hydrogen bonds are strengthening the interaction between surface and O_3 leading to its adsorption energy of -1.74 eV. We find that the presence of OH interferes with the adsorption of ozone on reduced $\{111\}$ surfaces by blocking the oxygen-deficient site which is considered to be the active site for ozone adsorption and decomposition.

4 Conclusions

This study explores the adsorption of H_2O and O_3 on various surfaces of CeO_2 and investigates their stability and binding properties. The results show that the stoichiometric $\{110\}$ and $\{100\}$ surfaces exhibits stronger binding with O_3 and weaker binding with H_2O , whereas the stable $\{111\}$ surface demonstrates slightly stronger binding with H_2O compared to O_3 . On the other hand, the $\{111\}$, $\{110\}$ and $\{100\}$ surfaces show strong binding with O_3 , particularly in the presence of oxygen vacancies. The preferred adsorption site on the stoichiometric CeO_2 surface is the Ce site, but on the reduced surface, the adsorbate either binds near an oxygen-deficient site or occupies it.

The presence of H-OH weakens the binding of O_3 , indicating water poisoning, and modifies its structure. O_3 forms a longer Ce-O bond when bound to the surface Ce atom, indicating a weaker

interaction and reduced electron transfer. The adsorption energy and geometrical parameters of O₃ remain unchanged when placed farther away from H-OH. There is minimal interaction between H₂O and O₃, meaning the presence of H₂O does not affect ozone adsorption.

The presence of OH reduces the negative adsorption energy of O₃, especially when oxygen vacancies are increased, leading to weaker ozone interaction. A fully hydroxylated surface prevents O₃ from forming chemical bonds with surface atoms, but hydrogen bonding between O₃ and hydrogen atoms provides stability.

In conclusion, this research highlights the importance of moisture control to prevent water poisoning and optimize the performance of CeO₂-based catalysts in industrial applications aimed at reducing ground-level ozone pollution. Heat treatment can be employed to reduce vacancy concentration, increase available adsorption sites for O₃, and minimize competitive adsorption by H₂O.

Acknowledgments

This work was supported financially by the Fundamental Research Program (PNK9400) of the Korea Institute of Materials Science (KIMS). The authors also acknowledge the support by the Korea Institute of Science and Technology, GKP (Global Knowledge Platform, Grant number 2V6760) project of the Ministry of Science, ICT and Future Planning.

References

- (1) Vatankhah, H.; Szczuka, A.; Mitch, W. A.; Almaraz, N.; Brannum, J.; Bellona, C. Evaluation of Enhanced Ozone–Biologically Active Filtration Treatment for the Removal of 1,4-Dioxane and Disinfection Byproduct Precursors from Wastewater Effluent. *Environ. Sci. Technol.* **2019**, *53*, 2720.

- (2) Camel, V.; Bermond, A. The use of ozone and associated oxidation processes in drinking water treatment. *Water Research* **1998**, *32*, 3208.
- (3) Kim, J.; Choe, Y. J.; Kim, S. H.; Lee, S.-C.; Bhattacharjee, S. Grasping periodic trend and rate-determining step for S-modified metals of metal sulfides deployable to produce OH via H₂O₂ cleavage. *Applied Catalysis B: Environmental* **2019**, *253*, 60–68.
- (4) Pak, G.; Salcedo, D. E.; Lee, H.; Oh, J.; Maeng, S. K.; Song, K. G.; Hong, S. W.; Kim, H.-C.; Chandran, K.; Kim, S. Comparison of Antibiotic Resistance Removal Efficiencies Using Ozone Disinfection under Different pH and Suspended Solids and Humic Substance Concentrations. *Environ. Sci. Technol.* **2016**, *50*, 7590.
- (5) Felzer, B. S.; Cronin, T.; Reilly, J. M.; Melillo, J. M.; Wang, X. Impacts of ozone on trees and crops. *Comptes Rendus Geoscience* **2007**, *339*, 784.
- (6) J. Weschler, C. *Indoor Air* **2000**, *10*, 269.
- (7) Sillman, S. The relation between ozone, NO_x and hydrocarbons in urban and polluted rural environments. *Atmospheric Environment* **1999**, *33*, 1821–1845.
- (8) R. Solomon, K. Effects of ozone depletion and UV-B radiation on humans and the environment. *Atmosphere-Ocean* **2008**, *46*, 185.
- (9) J. Hubbell, B.; Hallberg, A.; R. McCubbin, D.; Post, E. Health-Related Benefits of Attaining the 8-Hr Ozone Standard. *Environmental Health Perspectives* **2005**, *113*, 73.
- (10) Turner, M. C.; Jerrett, M.; Pope, C. A.; Krewski, D.; Gapstur, S. M.; Diver, W. R.; Beckerman, B. S.; Marshall, J. D.; Su, J.; Crouse, D. L.; Burnett, R. T. Long-Term Ozone Exposure and Mortality in a Large Prospective Study. *American Journal of Respiratory and Critical Care Medicine* **2016**, *193*, 1134.
- (11) Li, W.; Gibbs, G. V.; Oyama, S. T. Mechanism of Ozone Decomposition on a Manganese

- Oxide Catalyst. 1. In Situ Raman Spectroscopy and Ab Initio Molecular Orbital Calculations. *J. Am. Chem. Soc.* **1998**, *120*, 9041.
- (12) Mathew, T.; Suzuki, K.; Ikuta, Y.; Nagai, Y.; Takahashi, N.; Shinjoh, H. Mesoporous Ferrihydrite-Based Iron Oxide Nanoparticles as Highly Promising Materials for Ozone Removal. *Angewandte Chemie International Edition* **2011**, *50*, 7381.
- (13) Gong, S.; Li, W.; Xie, Z.; Ma, X.; Liu, H.; Han, N.; Chen, Y. Low temperature decomposition of ozone by facilely synthesized cuprous oxide catalyst. *New J. Chem.* **2017**, *41*, 4828–4834.
- (14) Dong, C.; Yang, J.-J.; Xie, L.-H.; Cui, G.; Fang, W.-H.; Li, J.-R. Catalytic ozone decomposition and adsorptive VOCs removal in bimetallic metal-organic frameworks. *Nature Communications* **2022**, *13*, 4991.
- (15) Dhandapani, B.; Oyama, S. Gas phase ozone decomposition catalysts. *Applied Catalysis B: Environmental* **1997**, *11*, 129.
- (16) Chen, H.; Stanier, C. O.; Young, C. A.; Grassian, V. H. A Kinetic Study of Ozone Decomposition on Illuminated Oxide Surfaces. *J. Phys. Chem. A* **2011**, *115*, 11979.
- (17) Roscoe, J. M.; Abbatt, J. P. D. Diffuse Reflectance FTIR Study of the Interaction of Alumina Surfaces with Ozone and Water Vapor. *J. Phys. Chem. A* **2005**, *109*, 9028.
- (18) Noei, H.; Qiu, H.; Wang, Y.; Löffler, E.; Wöll, C.; Muhler, M. The identification of hydroxyl groups on ZnO nanoparticles by infrared spectroscopy. *Phys. Chem. Chem. Phys.* **2008**, *10*, 7092.
- (19) Nanayakkara, C. E.; Larish, W. A.; Grassian, V. H. Titanium Dioxide Nanoparticle Surface Reactivity with Atmospheric Gases, CO₂, SO₂, and NO₂: Roles of Surface Hydroxyl Groups and Adsorbed Water in the Formation and Stability of Adsorbed Products. *J. Phys. Chem. C* **2014**, *118*, 23011.

- (20) Zhang, T.; Li, C.; Ma, J.; Tian, H.; Qiang, Z. Surface hydroxyl groups of synthetic α -FeOOH in promoting OH generation from aqueous ozone: Property and activity relationship. *Applied Catalysis B: Environmental* **2008**, *82*, 131.
- (21) Zhao, L.; Sun, Z.; Ma, J. Novel Relationship between Hydroxyl Radical Initiation and Surface Group of Ceramic Honeycomb Supported Metals for the Catalytic Ozonation of Nitrobenzene in Aqueous Solution. *Environ. Sci. Technol.* **2009**, *43*, 4157.
- (22) Wang, M.; Zhang, P.; Li, J.; Jiang, C. The effects of Mn loading on the structure and ozone decomposition activity of MnOx supported on activated carbon. *Chinese Journal of Catalysis* **2014**, *35*, 335.
- (23) Liu, Y.; Zhang, P.; Zhan, J.; Liu, L. Heat treatment of MnCO₃: An easy way to obtain efficient and stable MnO₂ for humid O₃ decomposition. *Applied Surface Science* **2019**, *463*, 374–385.
- (24) Yan, L.; Bing, J.; Wu, H. The behavior of ozone on different iron oxides surface sites in water. *Scientific Reports* **2019**, *9*, 14752.
- (25) Kresse, G.; Hafner, J. Ab initio molecular-dynamics simulation of the liquid-metal–amorphous-semiconductor transition in germanium. *Phys. Rev. B* **1994**, *49*, 14251.
- (26) Perdew, J. P.; Burke, K.; Ernzerhof, M. Generalized Gradient Approximation Made Simple. *Phys. Rev. Lett.* **1996**, *77*, 3865.
- (27) Blöchl, P. E. Projector augmented-wave method. *Phys. Rev. B* **1994**, *50*, 17953.
- (28) Nolan, M.; Parker, S. C.; Watson, G. W. The electronic structure of oxygen vacancy defects at the low index surfaces of ceria. *Surface Science* **2005**, *595*, 223.
- (29) Nolan, M.; Grigoleit, S.; Sayle, D. C.; Parker, S. C.; Watson, G. W. Density functional theory studies of the structure and electronic structure of pure and defective low index surfaces of ceria. *Surface Science* **2005**, *576*, 217.

- (30) Zhou, C.-Y.; Wang, D.; Gong, X.-Q. A DFT+U revisit of reconstructed CeO₂(100) surfaces: structures, thermostabilities and reactivities. *Phys. Chem. Chem. Phys.* **2019**, *21*, 19987.
- (31) Molinari, M.; Parker, S. C.; Sayle, D. C.; Islam, M. S. Water Adsorption and Its Effect on the Stability of Low Index Stoichiometric and Reduced Surfaces of Ceria. *J. Phys. Chem. C* **2012**, *116*, 7073.
- (32) Sims, J. R.; Blumenthal, R. N. *High Temp. Sci.* **1976**, *8*, 99.
- (33) Loschen, C.; Carrasco, J.; Neyman, K. M.; Illas, F. First-principles LDA + U and GGA + U study of cerium oxides: Dependence on the effective U parameter. *Phys. Rev. B* **2007**, *75*, 035115.
- (34) Shi, L.; Vathonne, E.; Oison, V.; Freyss, M.; Hayn, R. First-principles DFT+U investigation of charged states of defects and fission gas atoms in CeO₂. *Phys. Rev. B* **2016**, *94*, 115132.
- (35) Skorodumova, N. V.; Baudin, M.; Hermansson, K. Surface properties of CeO₂ from first principles. *Phys. Rev. B* **2004**, *69*, 075401.
- (36) Tasker, P. W. The stability of ionic crystal surfaces. *Journal of Physics C: Solid State Physics* **1979**, *12*, 4977.
- (37) Sayle, T. X. T.; Parker, S. C.; Catlow, C. R. A. Surface Segregation of Metal Ions in Cerium Dioxide. *J. Phys. Chem.* **1994**, *98*, 13625.
- (38) Balducci, G.; Kašpar, J.; Fornasiero, P.; Graziani, M.; Islam, M. S. Surface and Reduction Energetics of the CeO₂-ZrO₂ Catalysts. *J. Phys. Chem. B* **1998**, *102*, 557.
- (39) Fronzi, M.; Piccinin, S.; Delley, B.; Traversa, E.; Stampfl, C. Water adsorption on the stoichiometric and reduced CeO₂(111) surface: a first-principles investigation. *Phys. Chem. Chem. Phys.* **2009**, *11*, 9188–9199.
- (40) Watkins, M. B.; Foster, A. S.; Shluger, A. L. Hydrogen Cycle on CeO₂ (111) Surfaces: Density Functional Theory Calculations. *J. Phys. Chem. C* **2007**, *111*, 15337.

5 Tables and Graphics

Table 1: Structural parameters, adsorption energies ($E_{ads.}$), and Bader charges of O_3 adsorbed on CeO_2 surfaces. Oxygen atom of O_3 is represented by O_{ozone} .

Parameters	Free O_3	$CeO_2\{111\}$	$CeO_2\{110\}$	$CeO_2\{100\}$
$E_{ads.}$ (eV)	-	-0.40	-0.91	-1.04
$Q(O_3)(e)$	0	-0.25	-0.48	-0.72
$O_{ozone}-O_{ozone}$ (in Å)	1.28, 1.28	1.32, 1.29	1.33, 1.33	1.36, 1.36
O_3 bond angle ($^\circ$)	118.2	116.4	118.4	113.9
Ce- O_{ozone} (Å)	-	2.66	2.60	2.61-2.63

Table 2: Structural parameters, and adsorption energies ($E_{ads.}$) of O_3 on reduced CeO_2 surfaces. Oxygen atom of O_3 is represented by O_{ozone} .

Parameters	Free O_3	$CeO_2\{111\}$	$CeO_2\{110\}$	$CeO_2\{100\}$
$E_{ads.}$ (eV)	-	-3.24	-2.65	-2.71
$O_{ozone}-O_{ozone}$ (Å)	1.28, 1.28	1.54, 1.39	1.56, 1.39	1.44, 1.46
O_3 bond angle ($^\circ$)	118.2	109.0	110	110.2
Ce- O_{ozone} (Å)	-	2.29-2.51	2.33-2.77	2.40-2.54

Table 3: Adsorption energies ($E_{ads.}$) and structural parameters of H-OH and O_3 coadsorbed on $\{111\}$ surface of CeO_2 , when both are at a distance (d) of 2.54 Å and 6.34 Å from each other.

Parameters	H-OH	
	d = 2.54 Å	d = 6.34 Å
$E_{ads.}$ (eV)	-0.26	-0.38
$Q(O_3)(e)$	-0.20	-0.25
$Q(H-OH)(e)$	0.097	0.01
$O_{ozone}-O_{ozone}$ (Å)	1.33, 1.28	1.32, 1.29
O_3 bond angle ($^\circ$)	118.16	116.5
Ce- O_{ozone} (Å)	2.75	2.66

Table 4: Adsorption energies ($E_{ads.}$) and structural parameters of H₂O and O₃ coadsorbed on {111} surface of CeO₂, when both are at a distance (d) of 2.80 Å and 6.57 Å from each other.

Parameters	H ₂ O	
	d = 2.80 Å	d = 6.57 Å
$E_{ads.}$ (eV)	-0.36	-0.39
Q(O ₃)(e)	-0.25	-0.26
Q(H ₂ O)(e)	0.01	0.001
O _{ozone} -O _{ozone} (Å)	1.32, 1.29	1.32, 1.29
O ₃ bond angle (°)	115.4	116.40
Ce-O _{ozone} (Å)	2.70	2.66

Table 5: Adsorption energies ($E_{ads.}$) and structural parameters of OH and O₃ coadsorbed on {111} surface of CeO₂ at a vacancy concentrations x=0.0625 and 0.125.

Parameters	x=0.0625	x=0.125
$E_{ads.}$ (eV)	-0.58	-2.69
O _{ozone} -O _{ozone} (Å)	1.36, 1.36	1.47, 1.32
O ₃ bond angle (°)	114.24	111.4
Ce-O _{ozone} (Å)	2.45	2.58-2.83

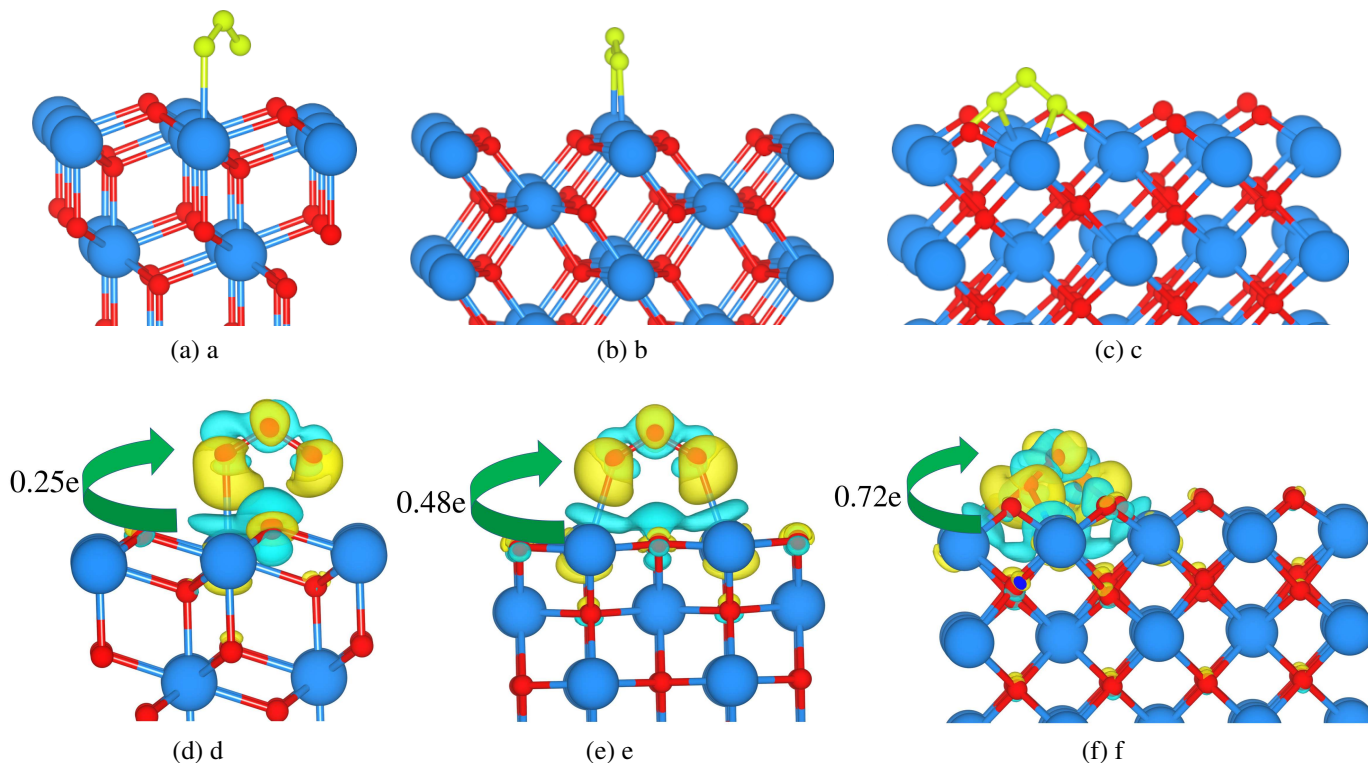


Figure 1: Stable binding configurations of O₃ on (a) {111}, (b) {110}, and (c) {100} CeO₂ surfaces. Charge density difference plot of O₃ interaction with (d) {111}, (e) {110}, and (f) {100} CeO₂ surfaces. The yellow and cyan color isosurfaces show charge accumulation and depletion respectively. Ce and O atoms are represented by blue and red color spheres respectively. O atoms of O₃ are shown by yellow spheres in order to distinguish it from the surface oxygen atoms. The direction of arrow shows the direction of electron transfer.

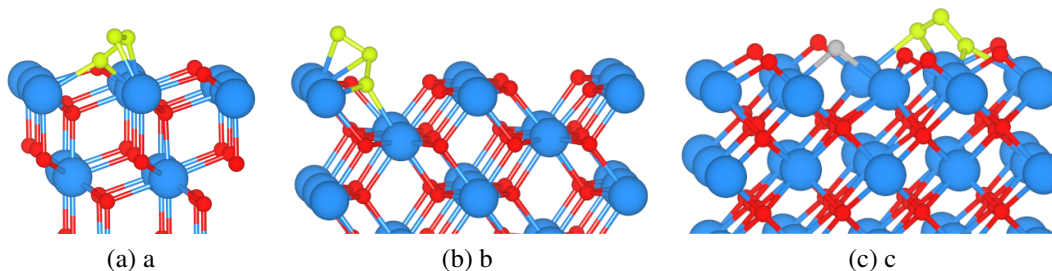


Figure 2: Adsorption of O₃ on reduced (a) {111}, (b) {110}, and (c) {100} surfaces of CeO₂. O₃ occupy the oxygen deficient site in {111} and {110} surfaces. Oxygen deficient site is represented by grey sphere.

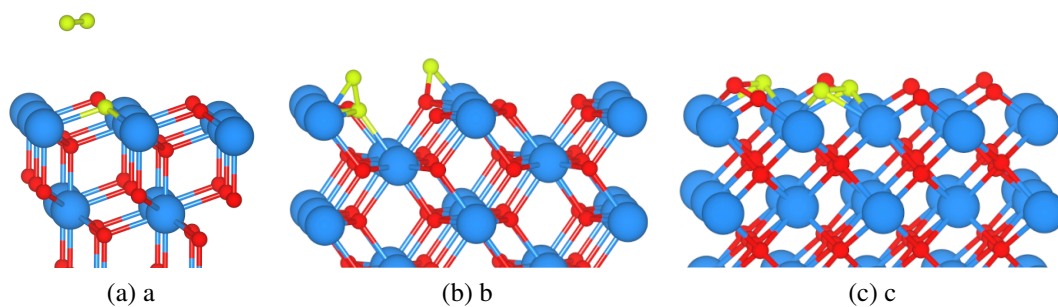


Figure 3: Dissociatively adsorbed O_3 on reduced (a) $\{111\}$, (b) $\{110\}$, and (c) $\{100\}$ surfaces of CeO_2 .

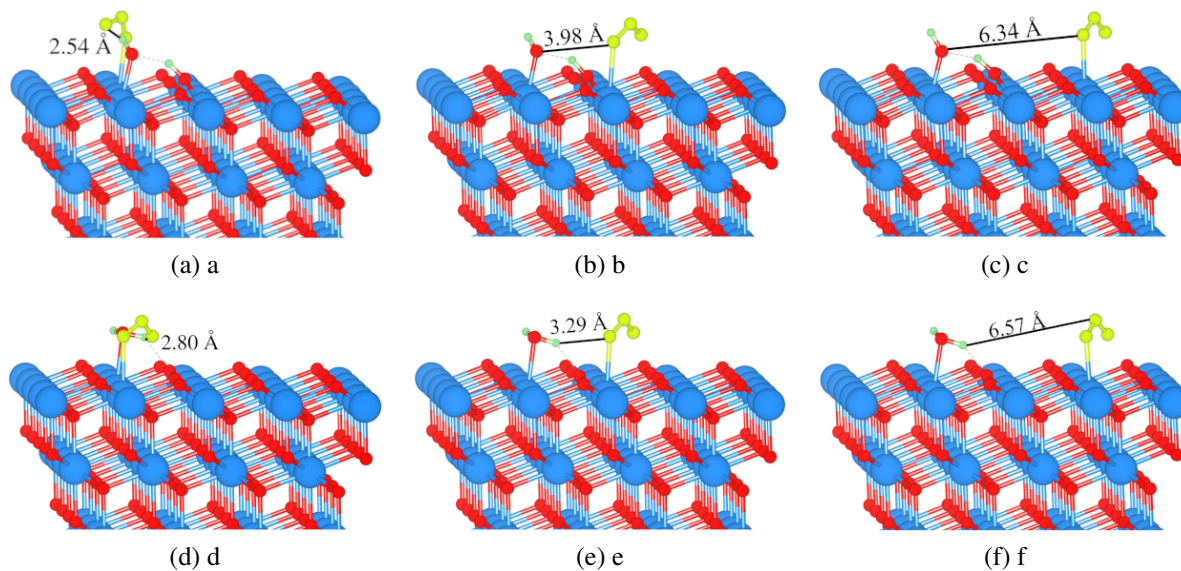


Figure 4: Structures of H-OH and O_3 (a)-(c) and H_2O and O_3 (d)-(f) on stoichiometric $CeO_2\{111\}$ surface, the black solid lines show the distance between H-OH/ H_2O and O_3 . Dotted lines are used to show hydrogen bond formation.

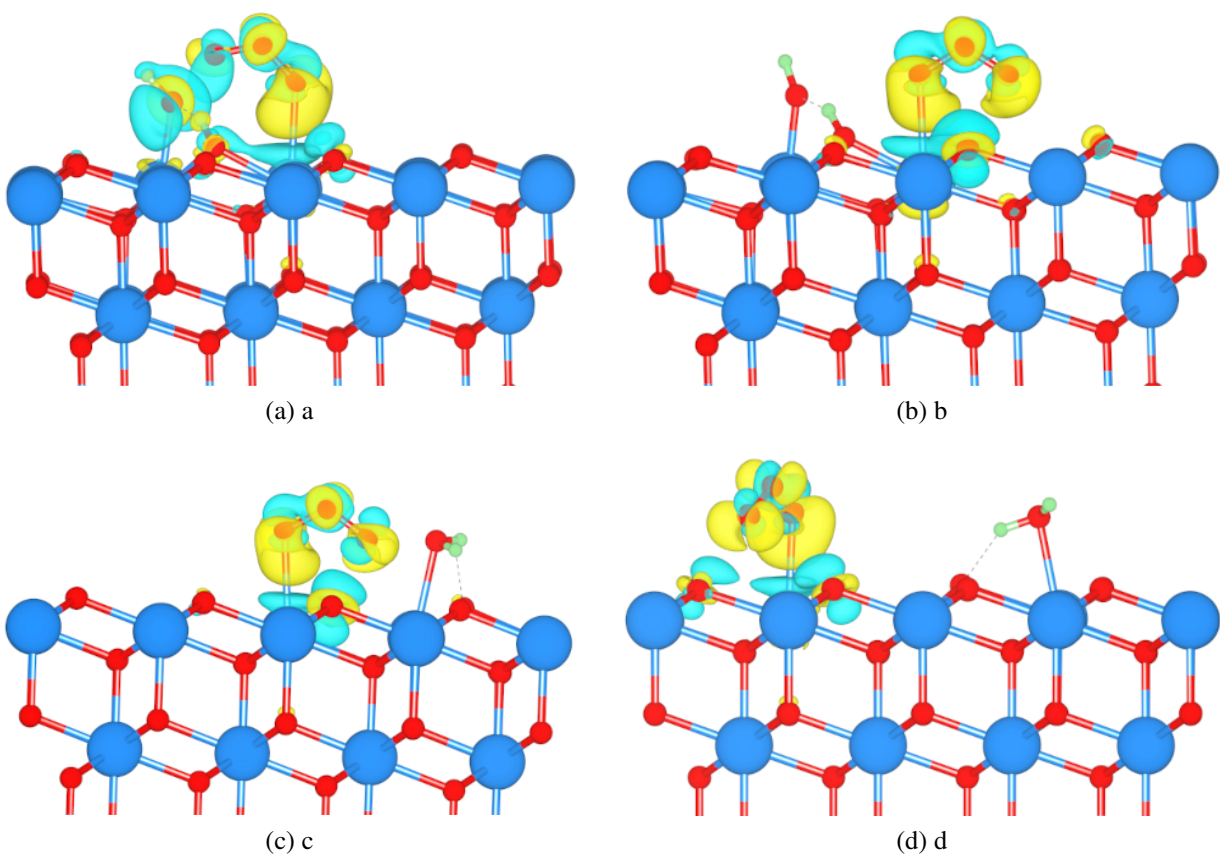


Figure 5: Charge density difference plots of O_3 interaction with $\{111\}$ surface of CeO_2 in the presence of H-OH when kept at a distance of (a) 2.54 Å, and (b) 6.34 Å from O_3 and when the distance between H_2O and O_3 is (c) 2.80 Å and (d) 6.57 Å. The yellow and cyan color isosurfaces show charge accumulation and depletion respectively.

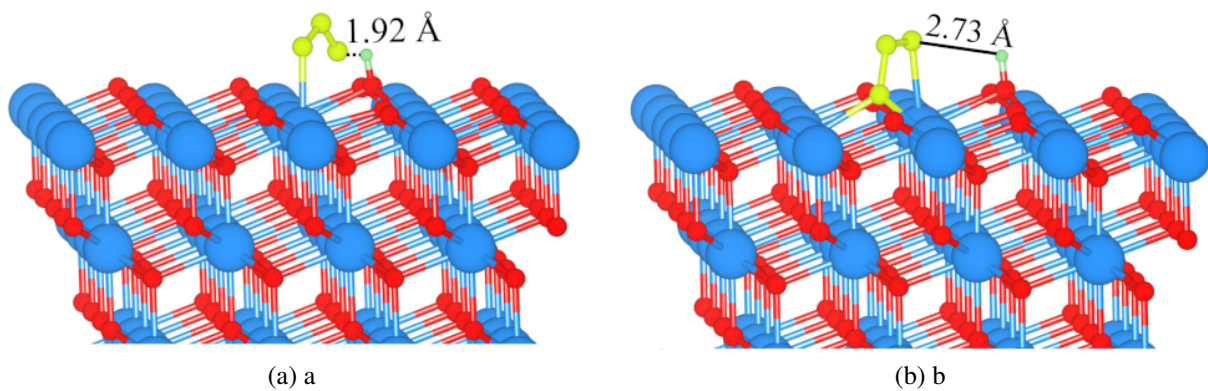


Figure 6: Stable binding configuration of OH and O_3 on the reduced $\{111\}$ CeO_2 surface for the vacancy concentration (a) 0.0625, and (b) 0.125. The dotted line shows the hydrogen bond.

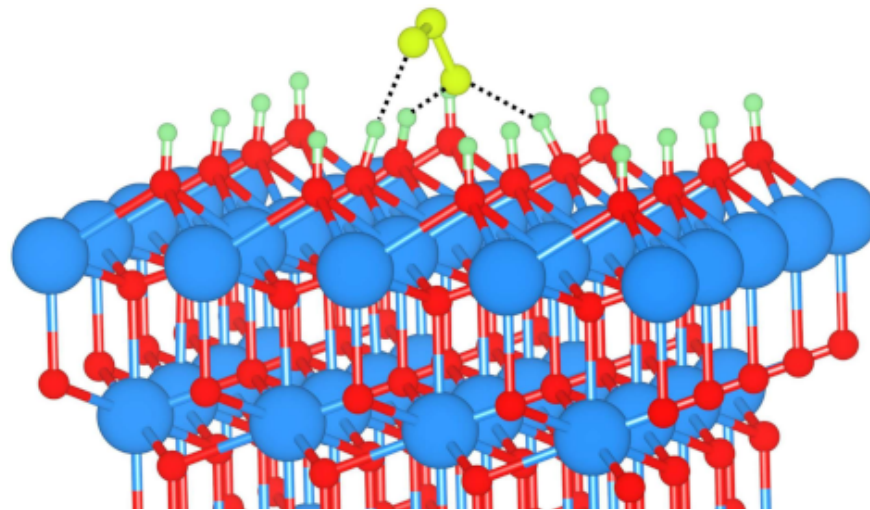


Figure 7: Stable binding configuration of O₃ on hydroxylated {111} surface. The dotted lines show the hydrogen bonds.